Received 27 April 2022; revised 7 June 2022; accepted 11 June 2022. Date of publication 16 June 2022; date of current version 24 June 2022.
The review of this article was arranged by Editor G. I. Ng

Digital Object Identifier 10.1109/JEDS.2022.3183638

Investigation on the Influence of Ohmic Structure on Channel-to-Channel Coupling Effect in InAlN/GaN Double Channel HEMTs

LING YANG [1] (Member, IEEE), HAO LU [1], MENG ZHANG [1], XUERUI NIU [1], CHUZHOU SHI [2], BIN HOU [1], MINHAN MI [1], MEI WU [1] (Member, IEEE), QING ZHU [1], YANG LU [1], LING LV [1], KAI CHENG [3], XIAOHUA MA [1] (Member, IEEE), AND YUE HAO [1] (Senior Member, IEEE)

1 State Key Discipline Laboratory of Wide Band-gap Semiconductor Technology, School of Microelectronics, Xidian University, Xi'an 710071, China
2 School of Advanced Materials and Nanotechnology, Xidian University, Xi'an 710071, China
3 Enkris Semiconductor Inc., Suzhou 215123, China

CORRESPONDING AUTHORS: M. ZHANG and B. HOU (e-mail: zhangmeng@xidian.edu.cn; bhou@xidian.edu.cn)

This work was supported in part by the National Natural Science Foundation of China under Grant 62090014; in part by the National Natural Science Foundation of China under Grant 62104184, Grant 62104178, Grant 62104179, and Grant 12035019; in part by the China National Postdoctoral Program for Innovative Talents under Grant BX20200262; and in part by the China Postdoctoral Science Foundation under Grant 2021M692499.

(Ling Yang and Hao Lu contributed equally to this work.)

ABSTRACT In this paper, the impact of ohmic structure on channel-to-channel (C2C) coupling effect in InAlN/GaN double channel (DC) HEMTs is systematically analyzed and studied. For the un-recessed ohmic structure, the electrons in the upper channel can easily inject into the bottom channel due to the ultra-thin InAlN back barrier layer. Therefore, the maximum drain current and transconductance peak of the bottom channel significantly increase. For recessed ohmic structure, the reduced vertical electric field strength of the upper channel can effectively weaken the coupling effect between the two GaN channels. Benefiting from the suppressed vertical transport of electrons in the upper channel, higher drain current and transconductance of the upper channel are obtained in the recessed ohmic structure. In addition, the transmission electron microscope (TEM) microstructural analysis of the DC HEMTs with recessed ohmic structure was also performed. This work shows that the recessed ohmic structure can modulate the electron transport mode in the InAlN/GaN DC HEMTs. The coupling effect of the two channels will play a major role in influencing the characteristics of current gain cutoff frequency (f_T) / maximum power gain cutoff frequency (f_{max}) versus V_{GS} and have a significant effect on large-signal characteristics, which is quite attractive for the fabrication of power microwave GaN-based HEMTs with wide gate swing.

INDEX TERMS GaN, InAlN/GaN double heterostructure, channel-to-channel coupling effect, recessed ohmic structure, RF characteristics.

I. INTRODUCTION

Gallium nitride (GaN) is an excellent choice for high power and robust electronics due to its wide bandgap and high critical electric field [1]–[5]. Another feature of GaN is its ability to be utilized in high electron mobility transistors (HEMTs) structures so that they can perform well in higher frequency applications such as radar and communication systems [6], [7]. AlGaN/GaN based double channel (DC) HEMTs have been explored to take advantage of two channels and higher current drive, which may have potential advantages in power switch devices [8] and RF circuit design [9]. On the one hand, GaN-based DC HEMTs could present a high mobility channel under the metal-oxide-semiconductor (MOS) field plate to allow a small series resistance in the Schottky barrier diode [10]. On the other hand, high current drive ability, good RF performance and gain linearity at high input power can all be realized when double-channel AlGaN/GaN HEMTs are designed with the InGaN back-barrier layer for the bottom channel and an AlGaN barrier layer for the upper channel [11]. Moreover,

This work is licensed under a Creative Commons Attribution-NonCommercial-NoDerivatives 4.0 License. For more information, see https://creativecommons.org/licenses/by-nc-nd/4.0/

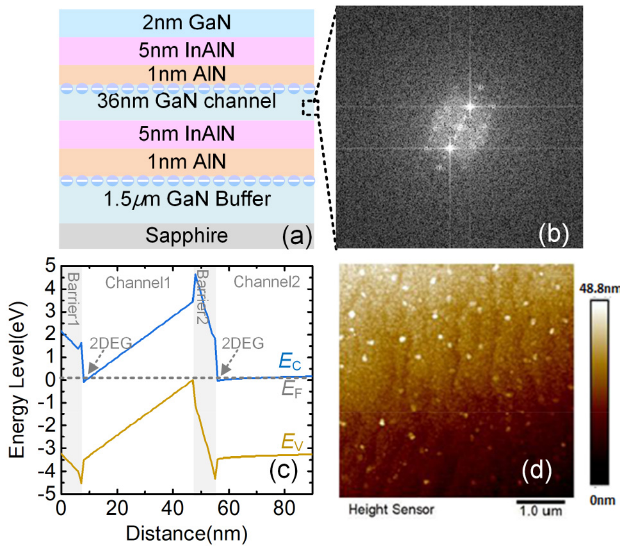

FIGURE 1. (a) Cross-section of ultra-thin InAlN barrier DC heterojunction. (b) FFT diffractogram of the GaN channel layer. (c) Corresponding energy band diagram of the InAlN barrier DC heterostructure. (d) Surface morphology with a scanned area of 5 µm × 5 µm.

the design of graded AlGaN:Si barrier layer between different channels allows tailing the access resistance to enhance the linearity of GaN-based transistors [12].

InAlN/GaN DC heterostructure [13], presenting an electron mobility of 1414 cm^2/Vs and carrier density of 2.55×10^{13} cm^{-2}, meets the needs of low sheet resistance and access resistance. This is a desirable feature for the high power and high frequency application. In order to further improve the gate control ability of the gate to the bottom channel, it is necessary to further reduce the InAlN spacer thickness between two channels. Due to a thin spacer layer, a strong channel-to-channel (C2C) coupling effect between the two channels occurs [14]. This effect reduces the on-resistance (R_{on}) in GaN-based DC HEMTs by exploiting both channels at the recess region while allowing currents to converge into the lower channel at the gate region. Until now, the electrostatics and transport characterization of thin InAlN barrier DC HEMT have not been comprehensively investigated yet. In this work, the strong C2C coupling effect was demonstrated in the ultra-thin InAlN barrier DC HEMT and the influence of ohmic structure on the electron coupling effect between two GaN channels was analyzed and discussed for the first time.

II. GROWTH EPITAXY AND DEVICE FABRICATION

Figure 1 (a) shows the cross-section of ultra-thin InAlN barrier DC heterojunction grown by MOCVD on a 3-inch sapphire substrate. The epi-structure consists of a 1.5 µm GaN buffer/transition layer, a 6 nm bottom barrier layer (including a 1 nm AlN, a 5 nm $In_{0.17}AlN$), a 36 nm GaN channel layer, a 6 nm upper barrier layer (including a 1 nm AlN, a 5 nm $In_{0.17}AlN$), and 2 nm GaN cap layer from bottom to top. The two dimensional electron gas (2DEG) induced by polarization is located at the upper GaN channel and the bottom GaN channel, respectively as shown in Fig. 1(a). It yields an electron mobility of 1432 cm^2/Vs, and a total 2DEG concentration of $1.35\times10^{13}cm^{-2}$, as is determined by Hall measurements. Figure 1 (b) shows the Fast Fourier transform (FFT) image of the GaN channel layer. Based on the clear crystalline structure of the FFT diffractogram, a high single crystalline quality of the epitaxial GaN channel layer was obtained and no phase separation of AlN and GaN was observed [15], [16]. Figure 1 (c) shows the corresponding energy band diagram of the InAlN barrier DC heterostructure, it can be seen that the two quantum wells under the Fermi-level indicate the double conduction channels formation. The sample surface morphology is shown in Figure 1 (d), which shows that the sample surface maintains step-flow morphology. The root mean square (RMS) roughness of InAlN/GaN double-channel heterojunction is approximately 1.2 nm with a scanned area of 5 × 5 μm^2.

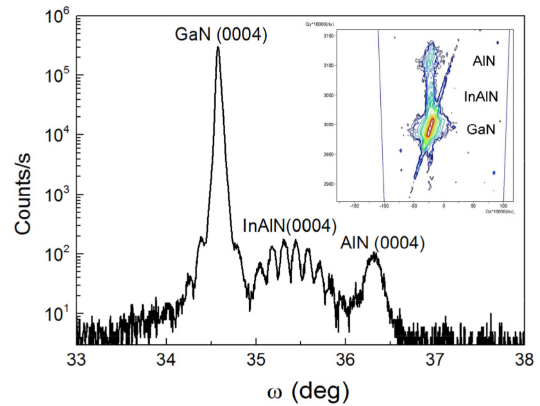

FIGURE 2. The inset is RSMs of the InAlN/GaN double channel structure.

Figure 2 shows the high-resolution X-ray diffraction (HR-XRD) ω-2θ scans rocking curves for (0004) reflection of InAlN/GaN double channel structure grown on sapphire. Three dominant peaks at around 35.7 °, 36.5 °, and 37.4 ° correspond to the GaN buffer layer (channel), InAlN barrier layer, and AlN nucleation layer, respectively. The indium mole fraction is 17% according to the Vegard's law, which makes the lattice constant of InAlN match with that of GaN. In addition, clearly diffraction fringes, which is general in superlattice structures, can be observed around the InAlN peak. This phenomenon is related to the multilayer characteristic of the double channel heterostructure, indicating the excellent interface quality. The inset figure in Figure 2 illustrates the reciprocal space maps (RSMs) of InAlN/GaN double channel structure. The narrowing in the RSM indicates a lower density of dislocations in InAlN/GaN double channel structures.

Device fabrication process started with mesa isolation by using Cl_2-based inductively coupled plasma (ICP). The drain/source-recessed regions defined by optical lithography were treated with Cl_2-based plasma to remove $In_{0.17}AlN/AlN/GaN$ layers. The etching depth is $\sim$ 44 nm

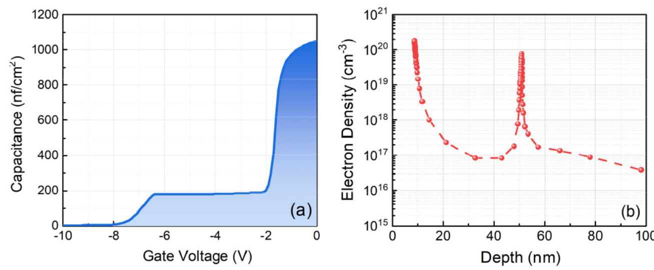

FIGURE 3. (a) Measured capacitance-voltage (C-V) characteristics and (b) electron distribution extracted from the C-V curves of Schottky barrier diode in ultra-thin InAlN/GaN double channel HEMTs.

measured by atomic force microscope (AFM). Ti/Al/Ni/Au metals were deposited and followed by rapid thermal annealing (RTA) at 830 °C for 30 s in N_2 environment. Conventional sample without the ohmic pre-etched was also fabricated. After the RTA process, the transmission line modeling (TLM) was performed to evaluate the contact resistance. The extracted contact resistance for the recessed ohmic contact sample and conventional sample were 0.38 and 0.40 Ω·mm, respectively, which indicates that the recessed ohmic contact has a slight improvement in terms of contact resistance. A SiN layer was deposited by Plasma Enhanced Chemical Vapor Deposition (PECVD) to serve as a passivation layer. The openings in the SiN layer were performed at the gate region. Then, Ni/Au e-beam evaporation and lift-off were carried out subsequently to form the gate pads. Circular-shaped Schottky barrier diodes (SBDs) with 130 μm gate diameter were used for capacitance-voltage (C-V) measurements and electron density profile evaluation. The devices with a gate length (L_G) of 0.5 μm, a gate width of 50 μm and source-drain spacing of 6 μm were used for the analysis of electrical performances and transport characteristics. Fat-FETs with $L_G = 50$ μm biased at linear region were used to derive the field mobility of electrons.

III. EXPERIMENTAL RESULTS AND DISCUSSION

The C-V characteristic of SBDs on the ultra-thin InAlN barrier DC heterostructure is shown in Figure 3. As can be seen from Figure 3(a), the two-step-like appearance of the two-channel heterostructure is obvious. Figure 3 (b) shows the distribution of electron density versus depth in ultra-thin InAlN barrier DC HEMTs calculated from the C-V plot. The method can be found in [17]. The electron density in the upper channel can achieve peak concentration up to 1.8×10^{20} cm^{-3} while that in the bottom channel can achieve peak concentration up to 0.45×10^{20} cm^{-3}.

To further investigate the microstructural properties of the recessed ohmic contact, scanning transmission electron microscopy (STEM) and energy-dispersive X-ray spectroscopy (EDS) were carried out. Figure 4(a) plots the HAADF-STEM imaging of the ohmic contact region for the recessed sample of DC heterostructure. Figure 4(b)-(h) depict the EDX mapping of Ti, Al, Ni, Au, In, Ga, and N

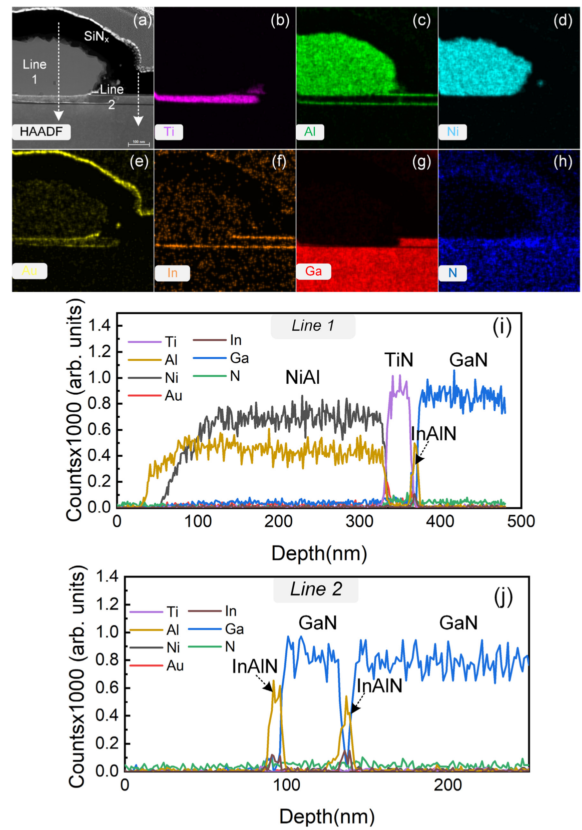

FIGURE 4. HAADF-STEM images of the recessed ohmic region for the double-channel heterostructure. (b)-(h) EDX elements mapping of Ti, Al, Ni, Au, In, Ga, and N present in the ohmic contact region. (i) - (j) EDS Line scan profile of line1-2 plotted in Fig. 4(a), respectively.

elements present in the ohmic contact region for the trenched sample. It can be seen that the TiN inclusions penetrated the upper GaN channel with the AlAu alloyed wrapping around. Hence, it has been proved that the double channels can form directly contact with the ohmic stack. In view of this, the electrons in the double channels can be simultaneously controlled. Figure 4(i)-(j) depict the elements distribution of Ti, Al, Ni, Au, In, Ga, and N elements along with the line 1-2 marked in Fig. 4(a), respectively. As demonstrated in Fig. 4(i), it can be further proved that the well-distributed TiN inclusions with the Au-Al alloys wraps around formed at the GaN channel layer [18], as well as the InAlN/GaN double channel heterostructure has been proved from Fig. 4(j).

Figure 5(a) and 5(b) shows the transfer characteristics of the ultra-thin InAlN barrier DC HEMTs with un-recessed ohmic structure and recessed ohmic structure, respectively. The distinct double-hump feature of the transconductance obviously reflects the direct current behavior, which corresponds to the bottom and upper 2DEG channels modulated by different gate voltages (V_{GS}). For the device with an un-recessed ohmic structure, there is larger hysteresis in the bottom channel during the gate double sweep. In the gate reverse sweep, the upper channel is in the off-state and only the access region of the upper channel can provide additional

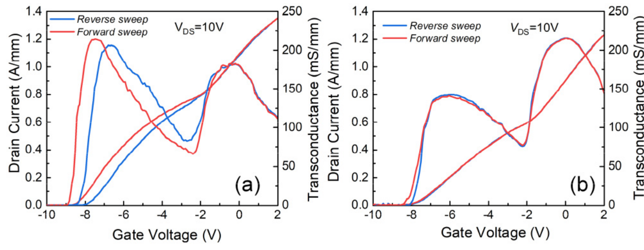

FIGURE 5. Measured linear-scale transfer characteristics in ultra-thin InAlN/GaN double channel HEMTs biased at drain voltage V_{DS} = 10V with (a) un-recessed ohmic structure and (b) recessed ohmic structure.

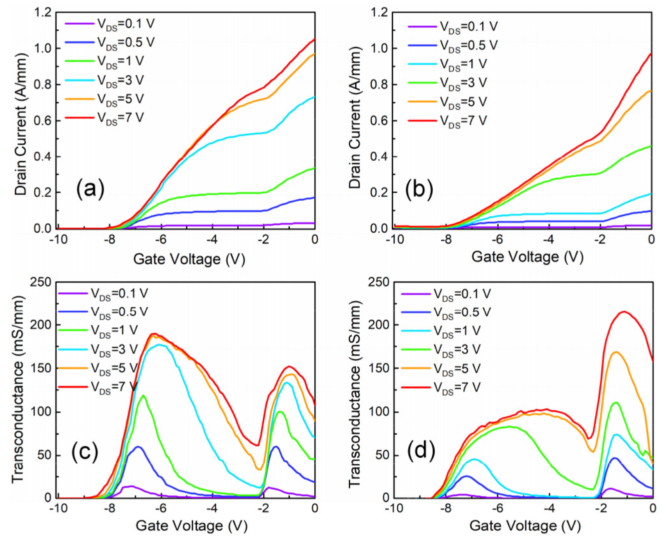

FIGURE 6. Measured linear-scale transfer characteristics in ultra-thin InAlN/GaN double channel HEMTs with different drain voltages in (a) un-recessed ohmic contact and (b) recessed ohmic contact. Transconductance curve in ultra-thin InAlN/GaN double channel HEMTs with different drain voltages in (c) un-recessed ohmic structure and (d) recessed ohmic structure.

injected electrons to the bottom channel. In the gate forward sweep, the upper channel is in the on-state and the whole upper channel can provide more additional injected electrons to the bottom channel. At this time, the bottom channel can provide more output current and then transconductance peak of the bottom channel is higher than that of the upper channel. It indicates that the current growth rate in the bottom channel exceeds the upper channel in the un-recessed ohmic structure. For the device with the recessed ohmic structure, there is no hysteresis in the transfer curve and the transconductance peak of the bottom channel is lower than that of the upper channel. It indicates that the coupling effect between the two channels is effectively suppressed.

To investigate the difference in transfer characteristics of the ultra-thin InAlN barrier DC HEMTs without/with recessed ohmic structure, multi-transfer curves under different drain voltages (V_{DS}) are measured and shown in Figure 6(a) and 6(b). At V_{DS} = 7 V, the drain currents of devices with the un-recessed and recessed ohmic structure are 1.05 and 0.97 A/mm, respectively. The device without the recessed ohmic structure has a higher saturation drain current than that with the recessed ohmic structure. It indicates that the coupling effect between two channels can increase the total drain output current.

Figure 6(c)-(d) shows the multi-transconductance curves with different drain voltages in ultra-thin InAlN barrier DC HEMTs with un-recessed ohmic structure and recessed ohmic structure. The transconductance profiles of the two kinds of devices are completely different. Due to the strong coupling effect between two GaN channels in the device with the un-recessed ohmic structure, a higher transconductance peak appears in the bottom channel and a lower transconductance peak appears in the upper channel. However, the device with the recessed ohmic structure shows different behaviors in transconductance. It has a lower transconductance peak in the bottom channel and a higher transconductance peak in the upper channel. It further confirms that the recessed ohmic structure can effectively suppress the coupling effect of two channels

Figures 7(a) and 7(b) distinguish the drain current of the bottom and upper channel at V_{GS} of 0 V extracted from Fig. 6(a) and 6(b) for the InAlN/GaN double channel HEMTs with/without recessed ohmic structure, respectively. When

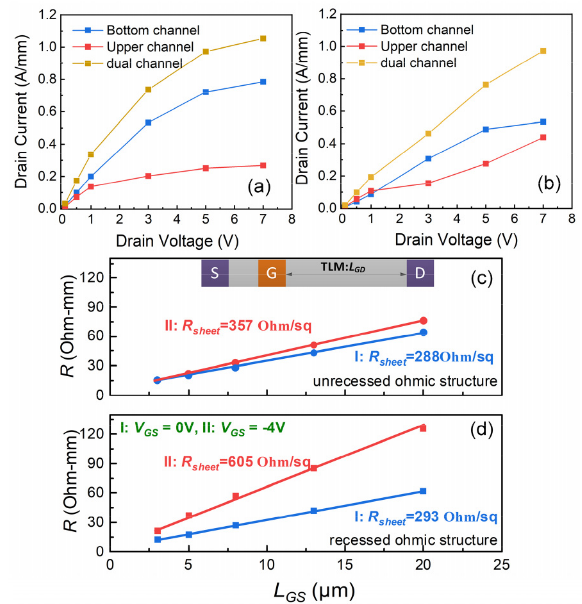

FIGURE 7. Extracted drain currents of the bottom and upper channel versus drain voltage at V_{GS} = 0V in ultra-thin InAlN/GaN double channel HEMTs with (a) un-recessed ohmic structure and (b) recessed ohmic structure. (c)-(d) Gated transmission line model (GTLM) characterizations on Schottky gate ultra-thin InAlN/GaN double channel HEMTs with L_{GD} as a variable.

the gate voltage increases from -10 to 0 V, the bottom channel and upper channel of the double-channel device are turned on gradually from bottom to top, as depicted in Fig. 6(a) and 6(b). The drain current of the dual-channel device increases at two different rates. In the first region (-8 V $< V_{GS} \leq -2$ V): the bottom channel turns on and

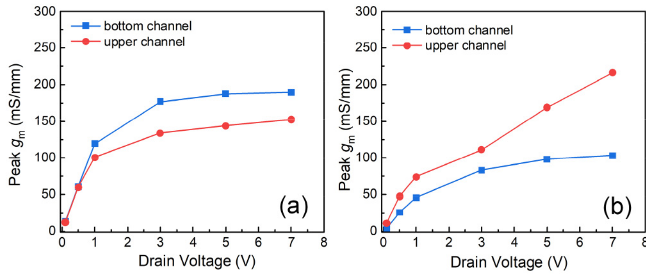

FIGURE 8. Measured peak of transconductance in the bottom and upper channels versus drain voltage in ultra-thin InAlN/GaN double channel HEMTs with (a) un-recessed ohmic structure and (b) recessed ohmic structure.

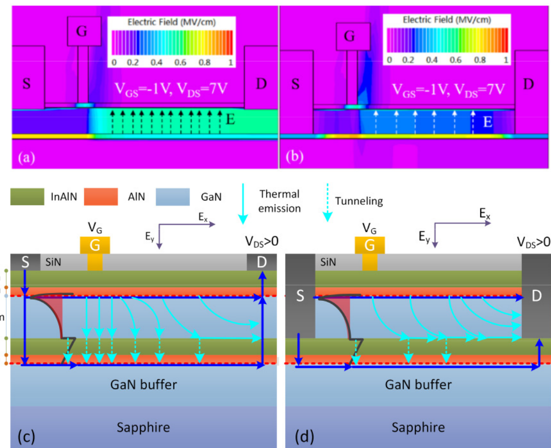

FIGURE 9. Electric field distribution at $V_{GS} = -1$ V and $V_{DS} = 7$ V for devices with (a) un-recessed ohmic structure and (b) recessed ohmic structure. Carrier transport mechanism between two GaN channel layers with (c) un-recessed ohmic structure and (d) recessed ohmic structure.

the upper channel pinches off. At this time, the drain current is completely supplied by the bottom channel. Therefore, we extract the drain current when the gate voltage is near -2 V as the maximum drain current of the bottom channel. The second region ($V_{GS} > -2$ V): The upper channel begins to turn on, and the channel current is provided by both the bottom channel and the upper channel. Therefore, the maximum drain current of the upper channel is the output current when the gate voltage is 0 V minus the drain current when the gate voltage is -2 V. Compared with the recessed ohmic structure, the un-recessed ohmic structure has a higher maximum output current and smaller on-resistances. For the un-recessed ohmic structure, the bottom channel has a smaller on-resistance and the maximum output current of the bottom channel is about three times larger than that of the upper channel (@$V_{DS} = 7$ V). For the recessed ohmic structure, the upper and bottom channels have similar on-resistance and the maximum output currents in values. It indicates that the coupling effect can reduce the channel parasitic resistance and increase the output current. The suppression of the coupling effect by the recessed ohmic structure will worsen the on-resistance and output current of the device.

To evaluate the C2C electrical coupling in the ultra-thin InAlN/GaN double channel heterostructures, Schottky gate TLM characterizations were performed on a series of the ultra-thin InAlN/GaN double channel HEMTs with no gate recess. Here two bias regions are defined by setting V_{GS}. In region I, both two channels are turned on and are exploited for conduction. In region II, only the bottom channel is turned on, so the conduction in the access region depends on the C2C coupling strength. From Figure 7 (c), the device with the un-recessed ohmic structure exhibits similar R_{sheet} values in the region I (288 $\Omega/\square$) and region II (357 $\Omega/\square$). On the contrary, the device with recessed ohmic structure exhibits a much smaller R_{sheet} value (293 $\Omega/\square$) in the region I than in region II (605 $\Omega/\square$). Therefore, the device with the un-recessed ohmic structure features strong C2C coupling while that with the ohmic structure features much weaker C2C coupling.

Figure 8(a) and 8(b) shows that the variation trend of transconductance peak with drain voltages of ultra-thin InAlN barrier DC HEMTs with the un-recessed ohmic structure and recessed ohmic structure. For the un-recessed ohmic structure, the transconductance peak exhibits a fast saturation trend with the increase of drain voltage both in the bottom channel and the upper channel. For recessed ohmic structure, the transconductance peak in the bottom channel has a smaller saturation peak compared with the un-recessed ohmic structure. Besides, the transconductance peak in the upper channel increases rapidly, especially at high drain voltage. It indicates that the ability of drain to collect electrons in the upper channel of device with the recessed ohmic structure is enhanced at high drain voltage.

Electric field distributions of devices with the un-recessed ohmic structure and recessed ohmic structure using TCAD simulation are shown in Figures 9 (a) and (b). The devices are biased at $V_{GS} = -1$ V and $V_{DS} = 7$ V. The electric field in the devices with the un-recessed ohmic structure is larger than that in devices with recessed ohmic structure. Due to the reduction of electric field strength by the recessed ohmic structure, the electric field strength in the upper channel is effectively weakened and the number of electrons injected into the bottom channel is greatly reduced. Based on the analysis above, we summarize the modulation mechanism of the recessed ohmic structure on the electron coupling effect between the two channels in the ultra-thin InAlN barrier DC HEMTs [shown in Figures 9 (c) and (d)]. The fundamental reason of C2C coupling modulation is the change of electron transport mode in the upper channel. For the un-recessed ohmic structure, vertical transport is dominant compared to lateral transport. For the recessed ohmic structure, the vertical transport of electrons in the upper channel is effectively suppressed and lateral transport is dominant.

The small-signal measurements were conducted using Keysight E8363 network analyzer. The system was calibrated using a short-open-load-through calibration standard [19].

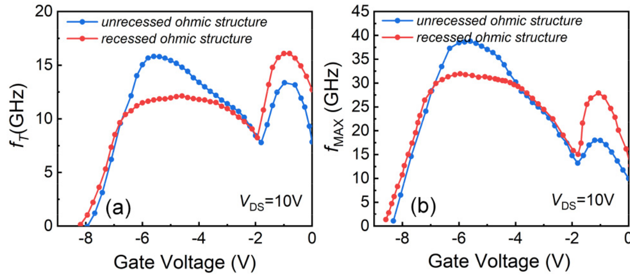

FIGURE 10. (a) f_T and (b) f_{max} of the ultra-thin InAlN/GaN double channel HEMTs with un-recessed ohmic structure and recessed ohmic structure.

The measured current gain cutoff frequency (f_T) and maximum power gain cutoff frequency (f_{max}) versus gate voltage at the bias of $V_{DS} = 10$ V. Figures 10 (a) and (b) show the gate voltage dependence values of f_T/f_{max} in the ultra-thin InAlN/GaN double channel HEMTs with the un-recessed ohmic structure and recessed ohmic structure. The f_T/f_{max} can be expressed as [20]:

$$f_T \approx \frac{g_m}{2\pi C_g} \tag{1}$$

$$f_{max} \approx \frac{f_T}{2\sqrt{\frac{R_i+R_s+R_g}{R_{ds}} + (2\pi f_T)R_g C_{gd}}} \tag{2}$$

where g_m is transconductance and C_g/C_{gd} is gate capacitance/gate-drain depletion capacitance, while R_i, R_s, R_g, and R_{ds} represent the gate-charging, source, gate, and output resistance, respectively. From equation (1), the curve of g_m versus V_{GS} determines the curve of f_T versus V_{GS}. Meanwhile, f_{max} has a positive correlation with f_T (from equation (2)). Thereby, the gate voltage dependence characteristic of f_{max} is similar to the transconductance curves biased at $V_{DS} = 10$ V with the un-recessed ohmic structure and recessed ohmic structure. However, the reduced R_{ds} caused by the turn-on of the upper channel when V_{GS} increases lead to the degeneration of f_{max}. It indicates that the coupling effect of the two channels will play a major role in influencing the characteristics of f_T/f_{max} versus V_{GS} and we can modulate the characteristics of f_T/f_{max} versus V_{GS} by recessed ohmic structure.

Figure 11(a) shows Mason's unilateral gain U against frequency for the ultra-thin InAlN/GaN double channel HEMTs with un-recessed ohmic structure and recessed ohmic structure at $V_{DS} = 20$ V and $V_{GS} = -5.7$ V/-1 V. Under the $V_{DS} = 20$ V and $V_{GS} = -5.7$ V, a high gain at 3.6 GHz is realized in the un-recessed ohmic structure (due to the high transconductance peak in the bottom channel), which is about 0.7 dB higher than that of the recessed ohmic structure. However, a high gain at 3.6 GHz under the $V_{DS} = 20$ V and $V_{GS} = -1$ V is realized in the recessed ohmic structure (due to the high transconductance peak in upper channel) which is about 0.5 dB higher than that of the un-recessed ohmic structure.

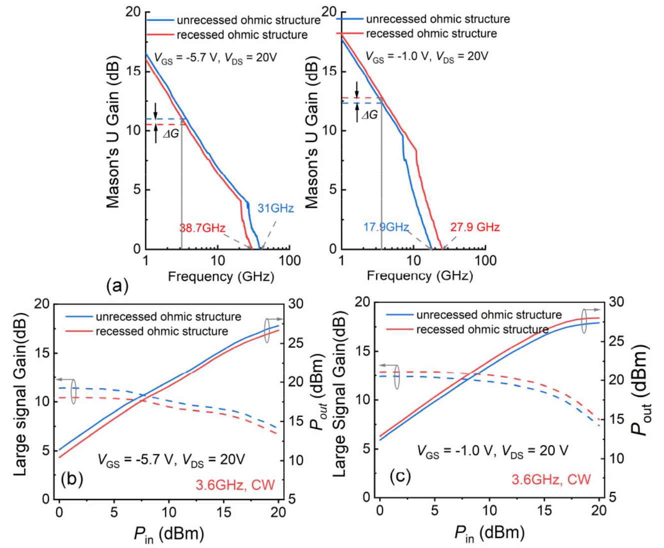

FIGURE 11. (a) Mason's unilateral gain U against frequency for the ultra-thin InAlN/GaN double channel HEMTs with un-recessed ohmic structure and recessed ohmic structure at $V_{DS} = 20$ V and $V_{GS} = -5.7$ V/-1 V. Continuous wave load-pull measurements of the ultra-thin InAlN/GaN double channel HEMTs with unrecessed ohmic structure and recessed ohmic structure bias at (b) $V_{GS} = -5.7$ V, $V_{DS} = 20$ V and (c) $V_{GS} = -1$V, $V_{DS} = 20$ V.

Figures 11 (b) and (c) depict the corresponding large-signal power performance of the un-recessed ohmic structure and recessed ohmic structure was measured at 3.6 GHz with the Maury load-pull system. The transistors for both samples were biased at the class-AB condition at $V_{DS} = 20$ V. Due to the high gain of the bottom channel (C2C coupling modulation) in un-recessed ohmic structure biased at $V_{GS} = -5.7$ V, the output power and associated gain have also been increased to 27.25 dBm and 7.25 dB, while for the recessed ohmic structure are 26.66 dBm and 6.67 dB, respectively. Owing to the high gain of the upper channel in recessed ohmic structure biased at $V_{GS} = -1$ V, the output power and associated gain have also been increased to 28.02 dBm and 8.01 dB, while for the un-recessed ohmic structure are 27.38 dBm and 7.39 dB respectively. It is observed that the ohmic structure in InAlN/GaN double channel HEMTs has a significant effect on large-signal characteristics and is quite attractive for the fabrication of wide gate swing power microwave GaN-based HEMTs.

IV. CONCLUSION

In summary, the impact of ohmic structure on the C2C coupling effect in ultra-thin InAlN barrier DC HEMTs is investigated in this work. The C2C coupling effect between two GaN channels can modulate the carrier transport mechanism. Vertical transport of electrons plays a leading role in the un-recessed ohmic structure, which results in high saturation current and small on-resistance. For devices with the recessed ohmic structure, the vertical field strength is reduced so that vertical transport of electrons is suppressed while lateral transport is dominant. The coupling effect of the two

channels influences a lot on the characteristics of f_T/f_{max} versus V_{GS} and the large-signal characteristics, which is quite attractive when target fabricating power microwave GaN-based HEMTs with wide gate swing.

REFERENCES

[1] Y. Wu, J. Gritters, L. Shen, R. P. Smith, and B. Swenson, "kV-class GaN-on-Si HEMTs enabling 99% efficiency converter at 800 V and 100 kHz," *IEEE Trans. Power Electron.*, vol. 29, no. 6, pp. 2634–2637, Jun. 2014, doi: 10.1109/TPEL.2013.2284248.

[2] Y. Hao *et al.*, "High-performance microwave gate-recessed AlGaN/AlN/GaN MOS-HEMT With 73% power-added efficiency," *IEEE Electron Device Lett.*, vol. 32, no. 5, pp. 626–628, May 2011, doi: 10.1109/LED.2011.2118736.

[3] L. Yang *et al.*, "Enhanced g_m and f_T with high Johnson's figure-of-merit in thin barrier AlGaN/GaN HEMTs by TiN-based source contact ledge," *IEEE Electron Device Lett.*, vol. 38, no. 11, pp. 1563–1566, Nov. 2017, doi: 10.1109/LED.2017.2757523.

[4] H. Lu *et al.*, "High RF performance GaN-on-Si HEMTs with passivation implanted termination," *IEEE Electron Device Lett.*, vol. 43, no. 2, pp. 188–191, Feb. 2022, doi: 10.1109/LED.2021.3135703.

[5] K. J. Chen *et al.*, "GaN-on-Si power technology: Devices and applications," *IEEE Trans. Electron Devices*, vol. 64, no. 3, pp. 779–795, Mar. 2017, doi: 10.1109/TED.2017.2657579.

[6] T. Palacios *et al.*, "High-power AlGaN/GaN HEMTs for Ka-band applications," *IEEE Electron Device Lett.*, vol. 26, no. 11, pp. 781–783, Nov. 2005, doi: 10.1109/LED.2005.857701.

[7] J. S. Moon *et al.*, "55% PAE and high power Ka-band GaN HEMTs with linearized transconductance via n+ GaN source contact ledge," *IEEE Electron Device Lett.*, vol. 29, no. 8, pp. 834–837, Aug. 2008, doi: 10.1109/LED.2008.2000792.

[8] J. Wei *et al.*, "Low on-resistance normally-off GaN double-channel metal–oxide–semiconductor high-electron-mobility transistor," *IEEE Electron Device Lett.*, vol. 36, no. 12, pp. 1287–1290, Dec. 2015, doi: 10.1109/LED.2015.2489228.

[9] S. K. Jha, C. Surya, K. J. Chen, K. M. Lau, and E. Jelencovic, "Low-frequency noise properties of double channel AlGaN/GaN HEMTs," *Solid-State Electron.*, vol. 52, no. 5, pp. 606–611, 2008, doi: 10.1016/j.sse.2007.10.002.

[10] J. Lei *et al.*, "650-V double-channel lateral schottky barrier diode with dual-recess gated anode," *IEEE Electron Device Lett.*, vol. 39, no. 2, pp. 260–263, Feb. 2018, doi: 10.1109/LED.2017.2783908.

[11] A. Kamath *et al.*, "Double-channel AlGaN/GaN high electron mobility transistor with back barriers," *IEEE Electron Device Lett.*, vol. 33, no. 12, pp. 1690–1692, Dec. 2012, doi: 10.1109/LED.2012.2218272.

[12] T. Palacios, A. Chakraborty, S. Heikman, S. Keller, S. P. DenBaars, and U. K. Mishra, "AlGaN/GaN high electron mobility transistors with InGaN back-barriers," *IEEE Electron Device Lett.*, vol. 27, no. 1, pp. 13–15, Jan. 2006, doi: 10.1109/LED.2005.860882.

[13] J. S. Xue, J. C. Zhang, Y. W. Hou, H. Zhou, J. Zhang, and Y. Hao, "Pulsed metal organic chemical vapor deposition of nearly latticed-matched InAlN/GaN/InAlN/GaN double-channel high electron mobility transistors," *Appl. Phys. Lett.*, vol. 100, no. 1, 2012, Art. no. 13507, doi: 10.1063/1.3675453.

[14] H. Lu *et al.*, "AlN/GaN/InGaN coupling-channel HEMTs for improved gm and gain linearity," *IEEE Trans. Electron Devices*, vol. 68, no. 7, pp. 3308–3313, Jul. 2021, doi: 10.1109/TED.2021.3082104.

[15] T. Takayama, M. Yuri, K. Itoh, T. Baba, and J. S. Harris, "Analysis of phase-separation region in wurtzite group III nitride quaternary material system using modified valence force field model," *J. Crystal Growth*, vol. 222, nos. 1–2, pp. 29–37, 2001, doi: 10.1016/S0022-0248(00)00869-1.

[16] T. T. Luong, Y.-T. Ho, Y.-Y. Wong, S. Chang, and E.-Y. Chang, "Phase separation-suppressed and strain-modulated improvement of crystalline quality of AlGaN epitaxial layer grown by MOCVD," *Microelectron. Rel.*, vol. 83, pp. 286–292, Apr. 2018, doi: 10.1016/j.microrel.2017.07.021.

[17] W. C. Johnson and P. T. Panousis, "The influence of debye length on the C-V measurement of doping profiles," *IEEE Trans. Electron Devices*, vol. 18, no. 10, pp. 965–973, Oct. 1971, doi: 10.1109/T-ED.1971.17311.

[18] H. Lu *et al.*, "Improved RF power performance of AlGaN/GaN HEMT using by Ti/Au/Al/Ni/Au shallow trench etching ohmic contact," *IEEE Trans. Electron Devices*, vol. 68, no. 10, pp. 4842–4846, Oct. 2021, doi: 10.1109/TED.2021.3101462.

[19] Q. Fan, J. H. Leach, and H. Morkoc, "Small signal equivalent circuit modeling for AlGaN/GaN HFET: Hybrid extraction method for determining circuit elements of AlGaN/GaN HFET," *Proc. IEEE*, vol. 98, no. 7, pp. 1140–1150, Jul. 2010, doi: 10.1109/JPROC.2010.2044630.

[20] S. M. Sze, *Physics of Semiconductor Devices*. New York, NY, USA: Wiley, 1981, pp. 342–343.